

*Short Communication*

## **Tribological Investigation of Nickel Nanocomposite Coated Piston Rings Reinforced with Multi-Walled Carbon Nanotubes**

*J S ShathishKumar<sup>1</sup> and A Jegan<sup>2</sup>*

<sup>1</sup> Department of Mechanical Engineering, VSA Group of Institutions, Salem-636010, Tamil Nadu, India

<sup>2</sup> Department of Mechanical Engineering, Sona College of Technology, Salem-636005, Tamil Nadu, India.

\*E-mail: [jssk189@gmail.com](mailto:jssk189@gmail.com)

*Received:* 12 December 2020 / *Accepted:* 6 February 2021 / *Published:* 28 February 2021

---

Piston ring is a vital mechanical element subjected to excessive wear and corrosion in any automotive application. This research work primarily focuses on investigating the tribological properties (wear resistance, corrosion and surface morphology) of nickel nanocomposite coated piston rings reinforced with multi-walled carbon nanotubes. Pulse reverse electroplating technique is employed for nano coating formulation. The required parameters are assessed with the aid of Vickers hardness, electrochemical impedance spectroscopy (EIS), scanning electron microscope (SEM), energy dispersive X – ray (EDX), X – ray diffraction (XRD), atomic force microscope (AFM) and coating thickness. From the results, it is evident that this particular coating formulation provides excellent tribological characteristics while compared with the uncoated one. Also, pulse reverse methodology technique provides uniform and better coating performance over complicated curved surfaces. The corrosion resistance of coated piston rings got an enhancement of about 25%, whilst an improvement of 84.5% is evidenced in the magnitude of microhardness value.

---

**Keywords:** Pulse reverse electroplating, Piston ring, Metal matrix nanocomposite, Microstructure, Microhardness, Corrosion.

### **1. INTRODUCTION**

Piston rings are usually subjected to extreme temperature operating conditions. In order to minimize the corrosion and wear characteristics, the surface is coated with additional materials like nickel and chromium.

Electrodeposition technique is proven to be the most economical one in coating metal matrix composites owing to its simple preparation, versatility, grain size and low temperature [1-2]. Co-

deposition technique is considered as an efficient technique to enhance the performance of coating parameters owing to the excellent mechanical and physical properties of composite materials [3-5].

Recent trends in coating technology have now turned its attention towards alternative techniques like pulse current (PC) and pulse reverse current (PRC) methodology for evidencing significant enhancement in electrodeposition rate which has direct impact over the corrosion, microstructure and mechanical properties [6-7]. Moreover, PRC method is proven to produce to high quality coatings with better surface morphology and corrosion resistance with lower structural defects [8-9]. This significant enhancement is evidenced due to the possible variation in pulse reverse parameters [10]. In addition, it produces superior coating with relatively large crystalline structure, higher reinforcement and smooth surface [11-12].

Applications of Carbon nanotubes (CNTs) have gained momentum in the recent years. Carbon nanotubes are considered to be the stiffest and strongest material due to their perfect atomic arrangement and high intrinsic strength. The carbon nanotubes possess excellent thermal conductivity, electrical conductivity, corrosion resistance and mechanical properties making it as suitable metal matrix reinforcement [13-15] and the contact surface is smoother due to less plastic deformation [16].

Nickel co-deposition coatings is broadly used on the coating surfaces of the metal substrates to enhance the properties like hardness, corrosion, wear, brightness and high temperature oxidation resistance [17-22]. Normally Ni-CNT nanocomposite coatings is smoother and its microhardness is twice than that of a normal nickel coating. The result of electrodeposition of Ni-CNT nanocomposite coatings provide super additive components for metal surface coatings [23].

The nanoparticles are considered as nano fillers for anti-corrosion surface coatings to increase the protection of corrosion performance [24-25]. In recent years, the EIS method has been generally used to study the corrosion behaviour and performance of protective coatings [26-30] and it is proven to be a powerful tool and also capable of providing significant results [31-35].

Although, numerous works were reported on literature in conjunction with pulse reverse current method and carbon nanotube coatings, Application of such kind of multi-walled carbon nanotubes (MWCNT) coatings on practical automotive application remains to be a vacuum domain for investigation. Based on the above facts, this present research work is focused to test the tribological performance and characteristics of nickel nano coated piston ring reinforced with multi-walled carbon nanotubes using pulse reverse electrodeposition method.

## 2. MATERIALS AND METHODS

Multi-walled carbon nanotubes (MWCNT) considered in this study is having a purity of 98 % and possess an average particle size of 16 nm. Ni-MWCNTs composite coatings are electrodeposited from Watts bath using pulsed reverse current on piston ring (Composition (%) : C- 2.6, Mn- 0.18, Si- 3.25, S- 0.012, P- 0.040, Cr- 0.14, Ni- 0.02, Mo- 0.01, Cu- 0.45 and Fe-Remaining) and (Microhardness – 336.6 Hv) substrate using a Dynatronix (USA) pulse power generator. Pure nickel (Ni) plate (99.9%) is used as the anode and a portion of piston ring is considered as the substrate for depositing Ni-MWCNT composite coatings. The piston ring is subjected to a pre-treatment process to facilitate removal of

unwanted impurities and ingredients. The compositions of Ni-MWCNT bath is listed in table 1 for reference.

**Table 1.** Materials used for coating.

Nickel Sulfate ( $\text{NiSO}_4 \cdot 6\text{H}_2\text{O}$ ) ( $\text{g L}^{-1}$ )	300
Nickel Chloride ( $\text{NiCl}_2 \cdot 6\text{H}_2\text{O}$ ) ( $\text{g L}^{-1}$ )	50
Boric Acid ( $\text{H}_3\text{BO}_3$ ) ( $\text{g L}^{-1}$ )	35
Sodyumdodecyl Sulfate (SDS) ( $\text{g L}^{-1}$ )	0.2
Coating reinforcement material (MWCNT) ( $\text{g L}^{-1}$ )	4
Temperature ( $^{\circ}\text{C}$ )	$50 \pm 2$
PH value	4
Anode	Nickel plate
Cathode	Piston ring (Substrate)

The pre-treated Ni-MWCNT compositions are added into a chemical plating bath containing 300 ml of distilled water solution with a fixed pH value of 4 and kept at a constant temperature of  $50^{\circ}\text{C}$ , thermostatically controlled with the aid of heater with mixer. The pulse reverse parameters of Ni-MWCNT composite coatings used in this study are following table 2 for reference [36-37].

**Table 2.** Coating method and parameters.

Method of coating	Pulse Reverse Electrodeposition (PRE)
Parameters	
Cathodic current density (CCD) ( $\text{A/cm}^2$ )	0.3 – 1.0
Cathodic current time (CCT) (s)	0.01
Anodic current density (ACD) ( $\text{A/cm}^2$ )	0.02 – 0.08
Anodic current time (ACT) (s)	0.02 – 0.1
Relaxation time (RT) (s)	0.1

The microstructure of the Ni-MWCNT nanocomposite coatings are examined using X-ray diffraction equipment (Rigaku-Japan-MiniFlex) using  $\text{Cu-K}\alpha$  radiation. The surface morphologies of the coatings is observed with scanning electron microscopy (Corel Zeiss – EVO 18). The microhardness of the Ni-MWCNT nanocoatings is tested by Vickers microhardness Shimadzu (HMV 2T indenter) tester. The reported values of microhardness values in the subsequent sections are taken with a load of 100

gram gradually applied over 15 seconds. The reported microhardness is the mean of the data taken at ten different geometrical locations.

The electrochemical performance of uncoated piston ring sample and Ni-MWCNT coated samples are tested with the aid of electrochemical impedance spectroscopy test (EIST) and potentiodynamic polarization kit (CH Instrument, Model 608 E). The measurement is carried out in three electrode modes using the piston ring as the working electrode and saturated calomel electrode (SCE) and platinum electrodes as reference and counter electrodes respectively, using one mole of sulphuric acid ( $\text{H}_2\text{SO}_4$ ) at a temperature of  $25\text{ }^\circ\text{C}$ .

The samples are covered completely with araldite resin except the coated surface area of about  $100\text{ mm}^2$ . Then each sample is immersed in the acid for one hour to determine the potentiodynamic polarization parameters ( $E_{\text{corr}}$ ,  $I_{\text{corr}}$ ,  $R_p$ ). Required curves and plots are generated by sweeping the electrodes in an open circuit potential ( $E_{\text{ocp}}$ ) of  $200\text{ mV}$  with the pair of anodic and cathodic directions sweeping at the rate of  $1.0\text{ mVs}^{-1}$ .

### 3. RESULTS AND DISCUSSION

#### 3.1 Microhardness

Sixteen samples of piston rings were coated using the parameters listed in table 2. Also from literature [37], it can be observed that better coating performance is achieved at higher cathodic current density (CCD) and lower anodic current density (ACD), anodic current time (ACT). Hence, the same protocol is extended for this study. Figure 2 clearly depicts the variation of the magnitude of microhardness (MH) at different process parameters. From the results it is evident that, higher cathodic current density and lower anodic current density yielded maximum value of microhardness [36-37]. Also, while compared with uncoated specimen, an increase of 84.5 % in the magnitude of microhardness is evidenced. The methodology and working mechanism of reverse current wave forms deployed in this study is illustrated in figure 1 for reference.

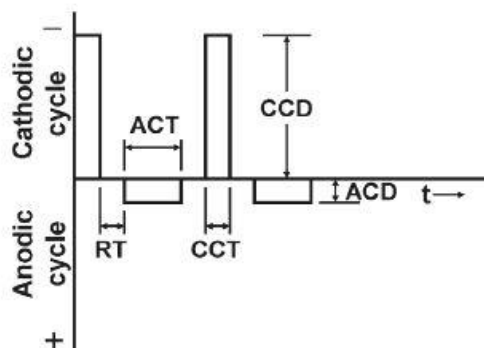


**Figure 1.** Working mechanism of pulse reverse current wave form.

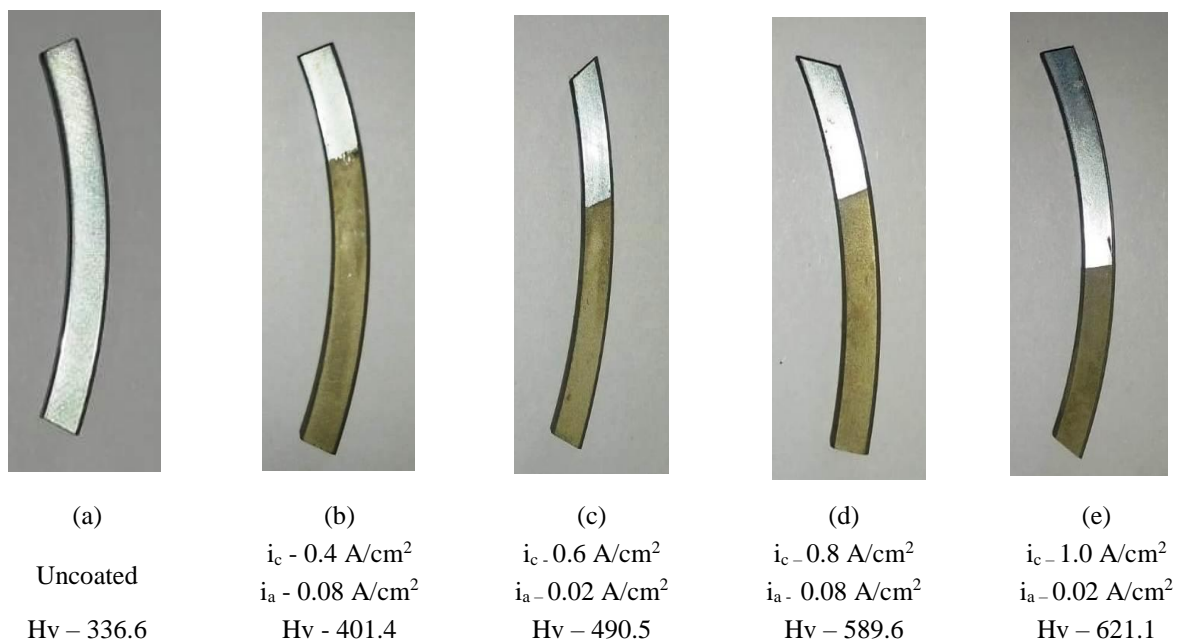


**Figure 2.** (a) Uncoated sample (b,c,d & e) Different combinations of PRC coating parameters with microhardness.

### 3.2. Potentiodynamic polarization

The final parameters ( $E_{corr}$ ,  $I_{corr}$ ,  $R_p$ ) of coated and uncoated piston ring samples are listed in table 3. Potentiodynamic polarization exploration is also performed and the curves are plotted in figure 3 for reference. From close observation it can be found that, the polarization resistance ( $R_p$ ) of Ni-MWCNT samples are far higher than the uncoated one which strongly signifies that Ni-MWCNT coated samples possess higher corrosion resistance characteristics [24 & 38]. This phenomenon is evidenced due to presence of multi-walled carbon nanotube (MWCNT) particles embedded into nickel (Ni) matrix. Also, the potentiodynamic polarization curves reflects the same result wherein a significant shift is seen between the samples.

**Table 3.** The results of potentiodynamic polarization test for uncoated piston ring sample and coated piston ring sample in nanocomposite coatings.

Sample	$E_{corr}$ (V)	$i_{corr}$ ( $\mu\text{A cm}^{-2}$ )	$R_p$ ( $\Omega \text{ cm}^2$ )
Uncoated piston ring	-0.558	0.6820	339
Ni-MWCNT coated piston ring	-0.513	0.1729	650

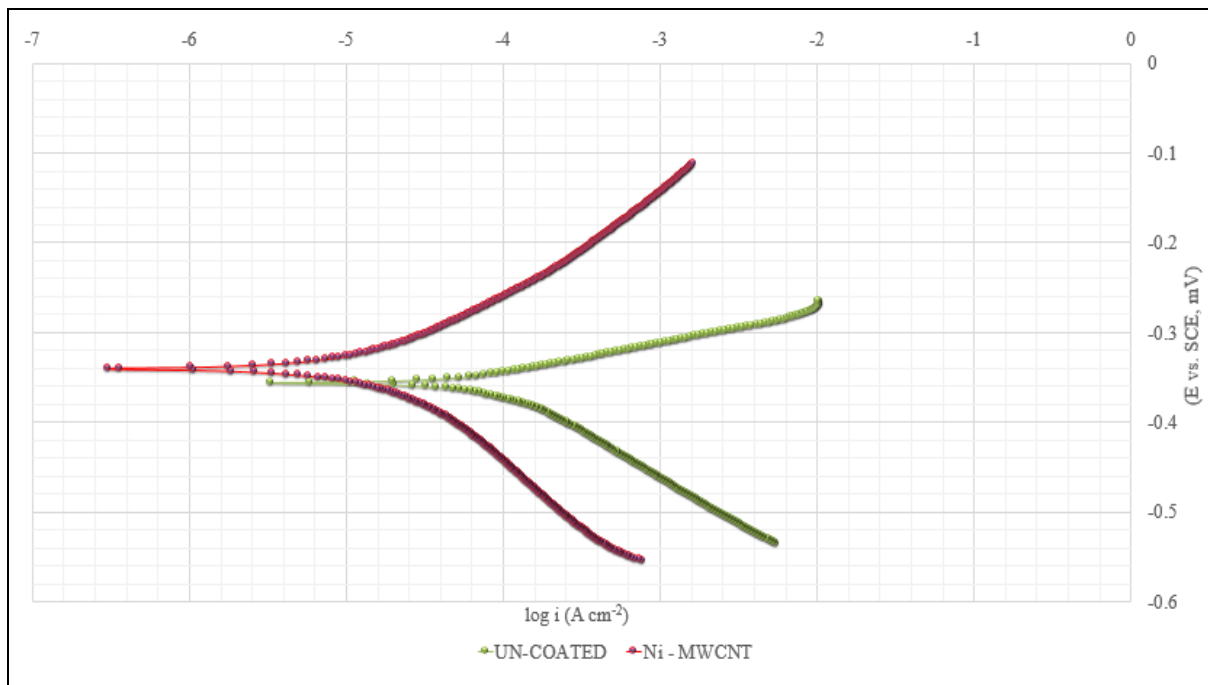


**Figure 3.** Potentiodynamic polarization curves of uncoated piston ring and coated piston ring in 1 M of H<sub>2</sub>SO<sub>4</sub>.

### 3.3. Electrochemical impedance spectroscopy test (EIST)

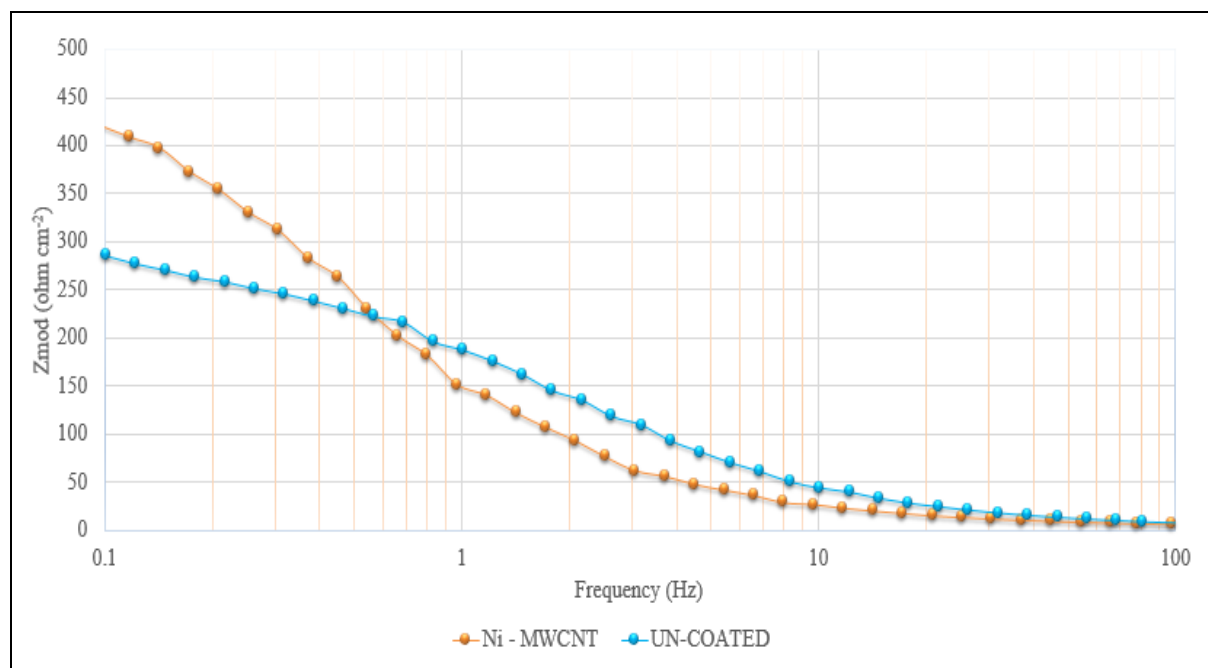


**Figure 4.** Bode impedance for uncoated piston ring and coated piston ring in 1 M of H<sub>2</sub>SO<sub>4</sub>.

To support and validate the results of potentiodynamic polarization, investigation of samples with electrochemical impedance spectroscopy test is also performed. Bode impedance plot and Nyquist

curves for the samples are depicted in figure 4 and 5 respectively. Bode impedance plot (Figure 4) reveals that, uncoated sample has a lower magnitude of impedance modulus. However, the variation with respect to time is almost similar for both the samples. From the Nyquist curve (Figure 5), it can be observed that the Ni-MWCNT coated sample bears higher curve radius which intern implies a better corrosion resistance [38]. Also, the life cycle of Ni-MWCNT coated samples will be high due to the increased magnitudes of real impedance modulus.

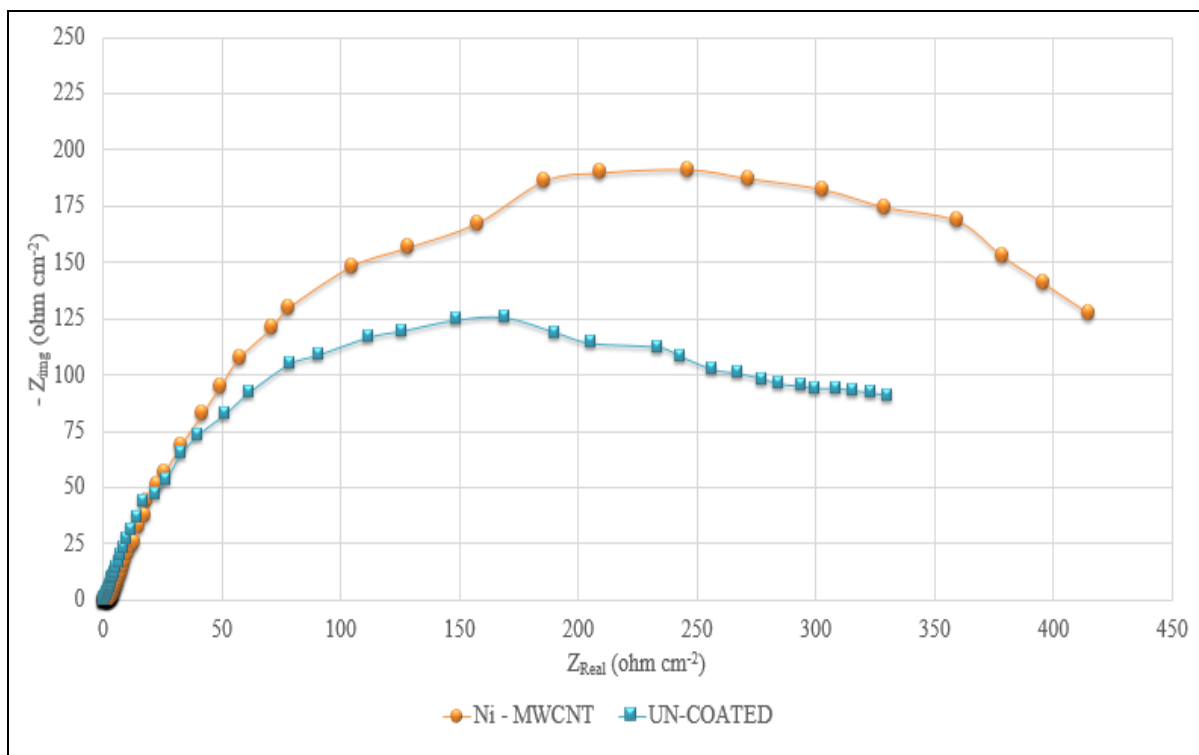


Figure 5. Nyquist impedance for uncoated piston ring and coated piston ring in 1 M of H<sub>2</sub>SO<sub>4</sub>.

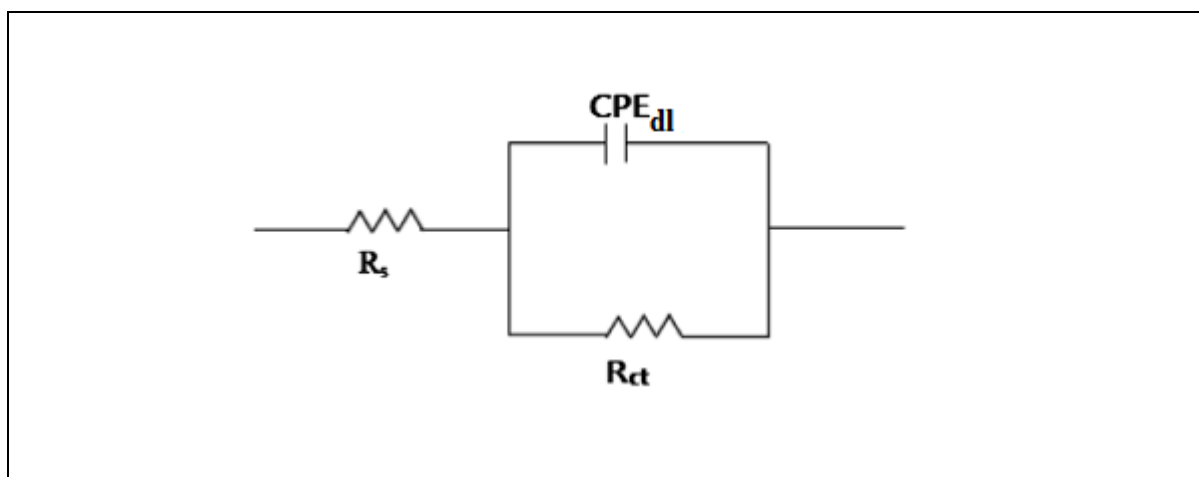


Figure 6. Equivalent circuit for uncoated piston ring and coated piston ring in 1 M of H<sub>2</sub>SO<sub>4</sub>.

An equivalent circuit is also modelled using the inbuilt simulation module and represented in figure 6. The parameters pertaining to the circuit for both the samples are highlighted in table 4 for clarity.

**Table 4.** Parameters fitted from EIST measurement.

Sample	$R_{ct}$ ( $\Omega \text{ cm}^{-2}$ )	$Y_o$ ( $\Omega^{-1} \text{ cm}^{-2} \text{ S}^{-n}$ )	n
Uncoated piston ring	366.3	0.0001391	0.8011
Ni-MWCNT coated piston ring	698.6	0.0004965	0.8656

### 3.4. Phase structure and surface morphology

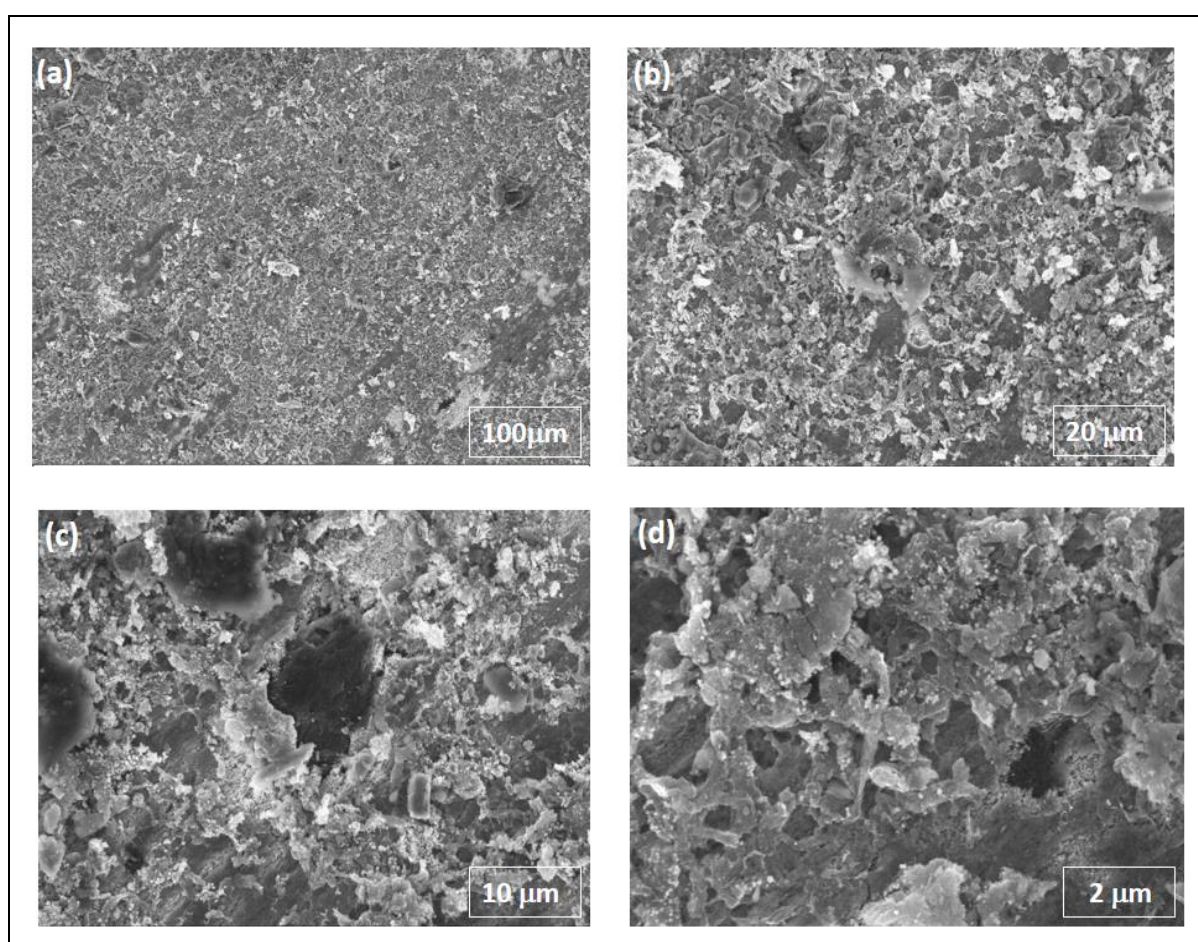


**Figure 7.** SEM micrographs of Ni-MWCNT

The influence and effect of multi-walled carbon nanotube (MWCNT) particles on the nickel (Ni) matrix is assessed with the aid of scanning electron microscopy (SEM), energy dispersive X-ray (EDX) and X-ray diffraction (XRD).

The scanning electron microscope images of Ni-MWCNT coated piston ring are shown in figure 7 at four different scales. From scanning electron microscope images, it can be seen that, multi-walled carbon nanotube particles are perfectly embedded into the pores of Ni composite matrix [39]. Bright regions represent nickel matrix in the images. Moreover, a uniform and even deposition rate is evidenced.

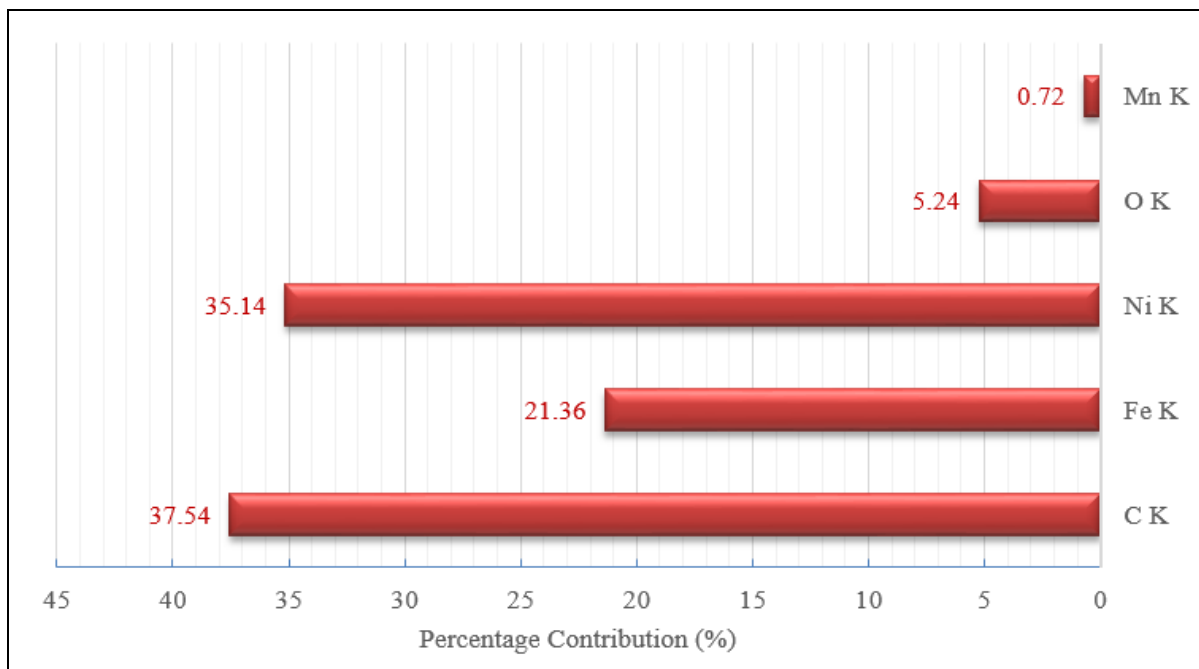


Figure 8. EDX of Ni-MWCNT

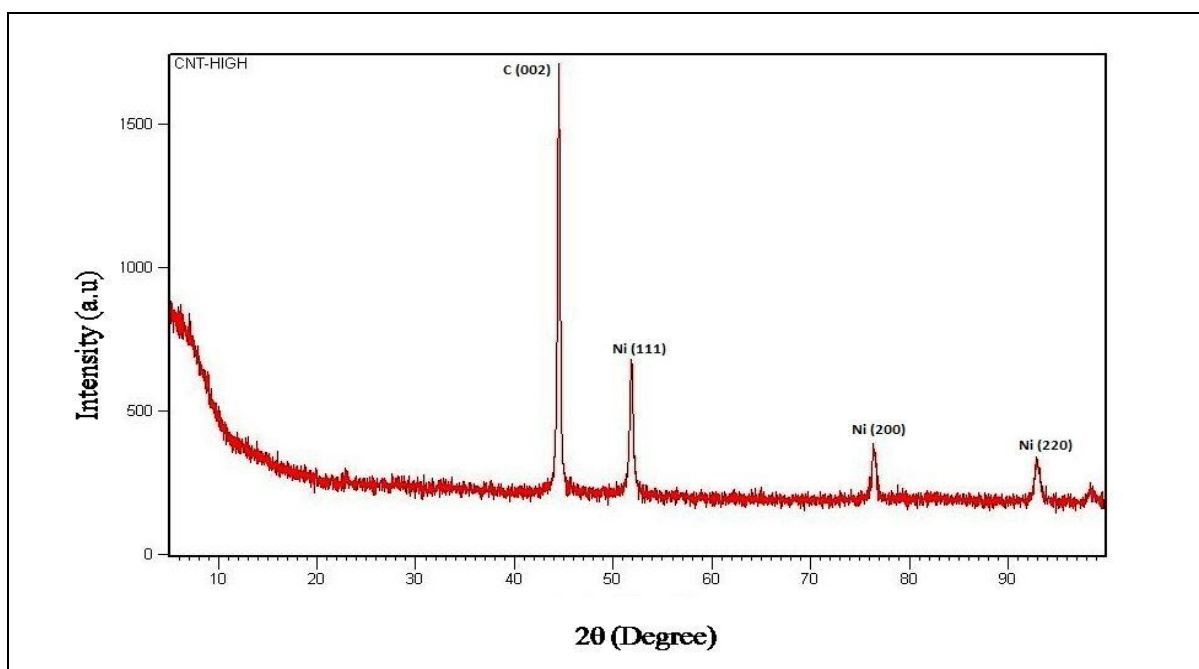
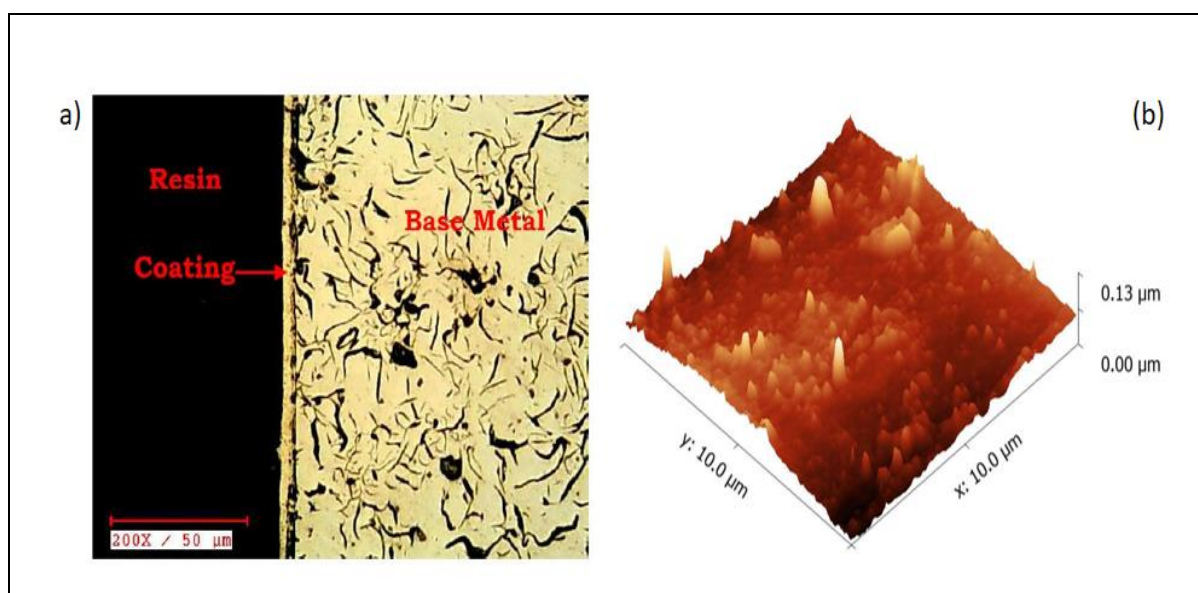


Figure 9. XRD pattern of Ni-MWCNT composite coating

Figure 8 represents the results of energy dispersive X-ray (EDX) experiment. The chemical compositions (Carbon (C K), Nickel (Ni K), Iron (Fe K), Oxide (O K) and Manganese (Mn K)) are listed clearly in figure 8. Due to the presence of carbon nanotube particles, the percentage of carbon content is higher and dominant. The natural phenomenon of carbon exhibits highly brittle characteristics which in turn produces excellent hardness.

The X-ray diffraction (XRD) pattern (Figure 9) indicates the (002), (111), (200) and (220) planes in presence of order to multi-walled carbon nanotubes and nickel composite coatings. However, Ni-MWCNT deposits exhibit a reinforcement at (002) plane due to carbon content with other planes comprising nickel crystallites [15].

### 3.5. Coating Thickness and Atomic force Microscope (AFM)



**Figure 10.** (a) Image of Ni-MWCNT coating thickness (b) AFM image of Ni-MWCNT coating

The coating thickness and deposition rate is investigated with a metallurgical microscope manufactured by Dewinter Tech. In order to ensure the accuracy of the final reported value, readings are taken at five different geometrical locations and the mean value is found to be 06 μm [37&40].

The surface morphology of the coated specimen is assessed with the aid of atomic force microscope (AFM). The average surface roughness value is 0.13 μm. However, for the same coating composition and parameters [37] on stainless steel specimen the magnitude of surface roughness was reported as 1.08 μm. Hence, it is evident that the composition and characteristics of base metal is dominant in deciding the surface roughness value. The sample images are exhibited in figure 10 (a) and (b) for reference.

#### 4. CONCLUSION

Ni-nano-MWCNT composite coating is electrodeposited on piston ring samples using pulse reverse electrodeposition technique. The tribological characteristics of the coated sample is superior in all aspects when compared with the uncoated one. Owing to the current demand in nanocomposite coatings, the significant findings of this research work can be utilized in various industrial applications where wear and corrosion is a dominant factor. Further works can be extended on various base metal samples with identical coating parameters to assess its performance.

#### Reference

1. M. Salehi, M. Mozammel and S.M. Emarati, *Colloids Surf. A: Physicochem Eng Asp.*, 573 (2019) 196–204.
2. D. Ning, A. Zhang, M. Murtaza and H. Wu, *J. Alloys Compd.*, 777 (2019) 1245–1250.
3. B. Ranjith and G.P. Kalaigan, *Appl. Surf. Sci.*, 257 (2010) 42–47.
4. F. Liu, Y. Deng, X. Han, W. Hu and C. Zhong, *J. Alloys and Compd.*, 654 (2016) 163–170.
5. F. Nasirpouri, *Electrodeposition of Nanostructure Materials, Springer Series in Surface Sciences* (2017).
6. M. Surender, R. Balasubramaniam and B. Basu, *Surf. Coat. Technol.*, 187 (2004) 93–97.
7. A. Balasubramanian, D.S. Srikumar, G. Raja, G. Saravanan and S. Mohan, *Surf. Eng.*, 25 (2009) 389–392.
8. M. Ramaprakash, S. Mohan and N.Rajasekaran, *J. Electrochem. Soc.*, 166 (2019) 145–150.
9. Z. He, D. Cao, Y. Wang, L. Yin, M.D. Hayat and H. Singh, *Surf. Eng.*, 36 (2020) 975–981.
10. M.H. Allahyarzadeh, M. Aliofkhaezadeh, A. Sabour Rouhaghdam and V. Torabinejad, *J. Alloys and Compd.*, 705 (2017) doi:10.1016/j.jallcom.2017.02.155
11. T. Frade, V. Bouzon, A. Gomes and M.I. da Silva Pereira, *Surf. Coat. Technol.* 204 (2010) 3592–3598.
12. D.D. Shreeram, V. Bedekar, S. Li, H. Cong and G. L. Doll, *JOM*, 70 (2018) 2603–2610
13. Z.L. An, M. Toda and T. Ono, *Compos. Part B: Eng.*, 95 (2016) 137–143.
14. E.J.T. Pialago and C.W. Park, *Appl. Surf. Sci.*, 308 (2014) 63–74.
15. M. Attarchi and S.K. Sadrnezhaad, *IJE Trans. B: App.*, 22 (2009) 161–168.
16. D. Ning, A. Zhang and H. Wu, *Materials*, 12 (2019) 392.
17. C. Liu, F. Su and J. Liang, *Trans. Nonferrous Met. Soc.*, 28 (2018) 2489–2498.
18. H. Zhou, Z. Liao, C. Fang, H. Li, F. Bin, S. Xu, G. Cao and Y. Kuang, *Trans. Nonferrous Met. Soc.*, 28 (2018) 88–95.
19. R. Arghavani, B. Bostani and N. Parvini-Ahmadi, *Surf. Eng.*, 31 (2015) 189–193.
20. V. Vitry, L. Bonin and L. Malet, *Surf. Eng.*, 34 (2018) 475–484.
21. Y. Bai, Z. Wang, X. Li, G. Huang, C. Li and Y. Li, *Materials*, 11 (2018) 853.
22. M.H. Nazir, Z.A. Khan, A. Saeed, V. Bakolas, W. Braun, R. Bajwa and S. Rafique, *Materials*, 10 (2017) 1225.
23. B.H. Thang, N.X. Toan and P.N. Minh, *Advances in Research*, 11 (3) (2019) 1–6.
24. A. Pruna, *Nanotechnology in Eco-Efficient Construction (Materials, Processes and Applications)*, (2019) 337–359. doi:10.1016/B978-0-08-102641-0.00015-3.
25. R.S. Prasannakumar, K. Bhakayaraj, V.I. Chukwuike, S. Mohan and R.C. Barik, *Surf. Eng.*, 35 (2019) 1021–1032.
26. Y. Zhang and Z. Guo, *J. Alloys. Compd.*, 724 (2017) 103–111.
27. E. Beltowska-Lehman, A. Bigos, P. Indyka, A. Chojnacka, A. Drewienkiewicz, S. Zimowski, M. Kot and M.J. Szczerba, *J. Electroanal. Chem.*, 813 (2018) 39–51.
28. A. Hefnawy, N. Elkhoshkhany and A. Essam, *J. Alloys. Compd.*, 735 (2017) 600–606.

29. J. Vega, H. Scheerer, G. Andersohn and M. Oechsner, *Corros. Sci.*, 133 (2018) 240–250.
30. H. Elmkhah, F. Attarzadeh, A. Fattah-alhosseini and K.H. Kim, *J. Alloys. Compd.*, 735 (2018) 422–429.
31. N. Imaz, M. Ostra, M. Vidal, J.A. Diez, M. Sarret and E. Garcia-Lecina, *Corros. Sci.*, 78 (2014) 251–259.
32. V. EzhilSelvi, H. Seenivasan and K.S. Rajam, *Surf. Coat. Technol.*, 206 (2012) 2199–2206.
33. S.H. Mosavat, M.H. Shariat and M.E. Bahrololoom, *Corros. Sci.*, 59 (2012) 81–87.
34. C.H. Lin and J.G. Duh, *Surf. Coat. Technol.*, 204 (2009) 784–787.
35. M. Lebrini, G. Fontaine, L. Gengembre, M. Traisnel, O. Lerasle and N. Genet, *Corros. Sci.*, 51 (2009) 1201–1206.
36. A.K. Pradhan and S. Das, *J. Alloys Compd.*, 590 (2014) 294–302.
37. J.S. ShathishKumar and A. Jegan, *Mater. Res. Express*, 7 (2020) 055012.
38. S. Ozkan, G. Hapci, G. Orhan and K. Kazmanli, *Surf. Coat. Technol.*, 232 (2013) 734–741.
39. M. Kartal, A. Alp and H. Akbulut, *IMMC*, 18 (2016) 844–847.
40. A. Jegan and R. Venkatesan, *Int. J. Miner. Metall. Mater.*, 20 (2013) 479–485.

© 2021 The Authors. Published by ESG ([www.electrochemsci.org](http://www.electrochemsci.org)). This article is an open access article distributed under the terms and conditions of the Creative Commons Attribution license (<http://creativecommons.org/licenses/by/4.0/>).